Applied Physics Letters

Ultrashort pulse chirp measurement via transverse second-harmonic generation in strontium barium niobate crystal

Cite as: Appl. Phys. Lett. **106**, 221108 (2015); https://doi.org/10.1063/1.4922144
Submitted: 23 December 2014 . Accepted: 23 May 2015 . Published Online: 05 June 2015

J. Trull, I. Sola, B. Wang, A. Parra, W. Krolikowski, Y. Sheng, R. Vilaseca, and C. Cojocaru

Ultrashort pulse chirp measurement via transverse second-harmonic generation in strontium barium niobate crystal

J. Trull,[1] I. Sola,[2] B. Wang,[1] A. Parra,[1] W. Krolikowski,[3,4] Y. Sheng,[3] R. Vilaseca,[1] and C. Cojocaru[1]

[1]*Departament de Física i Enginyeria Nuclear, Universitat Politècnica Catalunya, Terrassa 08222, Spain*
[2]*Grupo de Investigación en Óptica Extrema (GIOE), Departamento de Física Aplicada, Universidad de Salamanca, Plaza de la Merced s/n, 37008 Salamanca, Spain*
[3]*Laser Physics Centre, Research School of Physics and Engineering, Australian National University, Canberra ACT 0200, Australia*
[4]*Science Program, Texas A&M University at Qatar, Doha, Qatar*

(Received 23 December 2014; accepted 23 May 2015; published online 5 June 2015)

Pulse compression in dispersive strontium barium niobate crystal with a random size and distribution of the anti-parallel orientated nonlinear domains is observed via transverse second harmonic generation. The dependence of the transverse width of the second harmonic trace along the propagation direction allows for the determination of the initial chirp and duration of pulses in the femtosecond regime. This technique permits a real-time analysis of the pulse evolution and facilitates fast *in-situ* correction of pulse chirp acquired in the propagation through an optical system.
 [http://dx.doi.org/10.1063/1.4922144]

Ultrashort laser pulses, with their variety of peak powers and durations, are becoming an important tool in an increasing number of applications in the fields of technology (materials processing, etc.), biomedical sciences, and basic research, in general. As the pulses become shorter, the dispersion effects that modify pulse properties during propagation through optical materials become increasingly relevant so a precise characterization of the pulse properties is needed. During the last decade, different techniques have been implemented and extensively adopted[1–4] either for partial or/and complete temporal characterization of the pulses. They include, for instance, frequency-resolved optical gating (FROG, based on the concept of optical gating) or spectral phase interferometry for direct electric-field reconstruction (SPIDER, based on the concept of spectral interferometry), or even for 3D characterization (STARFISH, SEA Tadpole).[5,6] Although a detailed field reconstruction is needed in particular applications and thus fully justifies the use of these advanced techniques, there are still many situations requiring just a partial characterization of the pulse. Hence, simple and cost-effective methods of pulse measurement and characterization are always of potential interest.

Typical as-grown ferroelectric crystals, such as strontium barium niobate (SBN), exhibit a random-sized distribution of needle-like oppositely oriented ferroelectric domains all aligned parallel to the optical axis (z axis). A schematic representation of such domains is shown in Figure 1(a). While the reversed orientation of domains corresponds to inversion of sign of the quadratic susceptibility, the refractive index of these crystals remains practically homogeneous.[7] Such crystals provide phase matching for frequency conversion processes over wide angular and frequency bandwidths without need for angular or temperature tuning as it is usual in typically used homogeneous nonlinear crystals.[8–10] Phase matching is obtained thanks to the continuous set of reciprocal lattice vectors, G, arising from the random size and distribution of the nonlinear domains, which entails a random distribution of the nonlinearity sign. These lattice vectors, with different modulus and orientations, lie in the xy plane. As a result, planar second harmonic (SH) emission is observed when the input fundamental beam propagates in the direction perpendicular to the optical axis. This effect constitutes the so-called *transverse second harmonic generation* (TSHG) and is illustrated in Figure 1(b).

The implementation of a single-shot autocorrelation (AC) technique based on the recording of the TSHG due to noncollinear interaction of two replicas of the unknown pulse intersecting inside a nonlinear random crystal of SBN crystal has been recently demonstrated for pulses in the 200 fs range[11] from a Ti:sapphire oscillator with 5 nJ/pulse at 76 MHz repetition rate. In contrast to the traditional single shot AC setup[12] where the SH trace is recorded in the forward direction at the output of the nonlinear crystal, the TSHG captures the SH trace emitted in a lateral direction, at 90° with respect to the propagation direction of the input beams, and it allows for single-shot measurement of the AC trace as a function of the propagation distance inside the crystal. This measurement, combined with the known dispersion of the SBN crystal, makes possible the determination of the chirp of the incident pulse.

In this paper, we demonstrate the applicability of this method to measure pulse duration and linear chirp for ultrashort pulses of the order of 30 fs. The simplicity and easy implementation of the measuring elements allows for a real time control of the chirp content of the pulse at any desired position within an experimental setup.

In our experimental setup, two replicas of the beam to be measured propagate in the x-z plane of a SBN crystal forming angles $+\alpha$ and $-\alpha$ with respect to the x-axis. The nonlinear interaction inside the crystal of the two beams gives rise to three well-differentiated TSHG signals (Figure 1(c)). Two of them correspond to the conical SH emission from each individual beam. The third one, which results from the noncollinear interaction between the two beams in

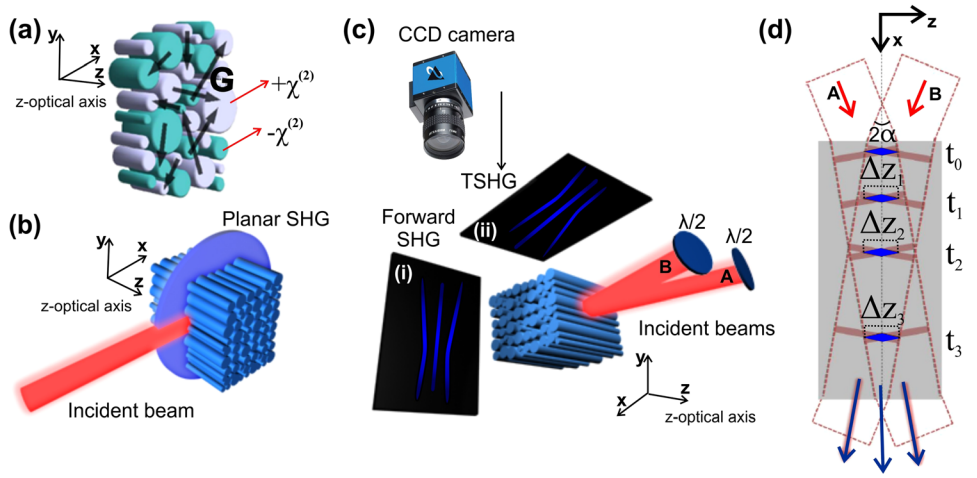

FIG. 1. (a) Schematic representation of the inverted random nonlinear domain distribution in the x-y plane of a SBN crystal showing the orientation of the reciprocal lattice vectors, (**G** vectors), in the xy plane. (b) TSHG scheme with the incident field propagating perpendicularly to the optical axis (z axis) of the crystal. (c) Noncollinear interaction of two incident beams ($\lambda = 790$ nm) crossing along x-y plane generating SH signal ($\lambda = 395$ nm) in both forward (i) and transverse (ii) directions. The central line in both images corresponds to planar SH emission with photons from each beam contributing to the SH signal; the other ones represent the conical emission from each individual incident beam. (d) Non-collinear interaction of both incident pulses inside SBN crystal, resulting in the AC TSHG signal.

the area where the pulses overlap, is emitted in the plane transverse to the optical axis and represents the transverse single-shot AC signal, as shown in Figure 1(d). This TSHG signal is recorded with a CCD camera placed at the top of the crystal. The width of this AC trace, Δz, is directly related to the pulse duration. Assuming a Gaussian beam profile of the input pulses, the intensity of the AC signal is given by the expression[9]

$$I_{2\omega}(z) = I_{o,2\omega} \exp\left(-\frac{2z^2 \sin^2(\alpha)}{u^2 T^2}\right), \tag{1}$$

where $u = c/n$ is the speed of light inside the crystal, T is the pulse duration measured at 1/e in intensity, α is the propagation angle of each beam inside the crystal, and z is the transverse direction. The expression for the pulse duration at FWHM in intensity, τ, is obtained directly from the value of the transverse width of the AC trace measured at FWHM, Δz_{FWHM}, as

$$\tau = \frac{\sqrt{2}\Delta z_{FWHM} \sin(\alpha)}{u} = \frac{\sqrt{2}\Delta z_{FWHM} \sin(\alpha_{ext})}{c}, \tag{2}$$

where α_{ext} corresponds to the incidence beam angle with respect to the x axis measured outside the crystal.

The initial pulse duration is modified during propagation in SBN due to the effect of material dispersion, characterized by the group velocity dispersion (GVD) coefficient $g = (\partial^2 k/\partial\omega^2)$. Therefore, the dependence of the AC trace width, Δz, with propagation distance, x, allows the measurement of additional properties such as the initial chirp. In this paper, we deal mainly with Gaussian pulses, $E(t) = E_o(t)\exp(-i\omega_o t)$, with

$$E_0(t) = Ae^{-\frac{t^2}{2T^2}} e^{-i\varphi(t)}; \quad \varphi(t) = \varphi_0 + \varphi_1 t + \frac{1}{2}\varphi_2 t^2 + \cdots, \tag{3}$$

where A is the amplitude of the pulse, ω_o is central frequency, T is the pulse duration (1/e in intensity) and $\varphi(t)$ is the temporal phase. A non-vanishing phase results in larger time-bandwidth product. In general, a pulse with phase modulation is longer than a Fourier transform limited pulse with the same spectrum.[13] The second order term φ_2 gives an instantaneous frequency, $\omega_{inst}(t) = \omega_o + d\varphi(t)/dt$, which varies linearly with time and results in up-chirped (if $\varphi_2 > 0$) or down-chirped ($\varphi_2 < 0$) pulses. Higher order contributions lead to pulse distortions. The pulse can be alternatively expressed in the spectral domain, through a Fourier transform of the temporal envelope, in terms of the frequency $\Omega = \omega - \omega_o$

$$\tilde{E}_o(\Omega) = \int E_o(t) e^{i\Omega t} dt = \tilde{A}(\Omega) e^{-i\tilde{\varphi}(\Omega)};$$
$$\tilde{\varphi}(\Omega) = \tilde{\varphi}_o + \tilde{\varphi}_1 \Omega + \frac{1}{2}\tilde{\varphi}_2 \Omega^2. \tag{4}$$

The coefficient $\tilde{\varphi}_2$ of the spectral phase term varying quadratically with Ω is the group delay dispersion (GDD).

Defining the pulse chirp parameter at the entrance of the crystal as $C = \varphi_2 T_o^{-2}$, where T_0 is the pulse duration (1/e in intensity) at the entrance of the crystal, the evolution of the pulse duration during propagation is given by the expression (valid up to second order in dispersion, i.e., for negligible third-order effects)[13]

$$T^2(x) = T_o^2 \left(1 + \frac{2sign(g)C}{L_D} x + \frac{1 + C^2}{L_D^2} x^2\right), \tag{5}$$

where $L_D = T_o^2/|g|$ is the GVD length over which the pulse duration increases by a factor of $\sqrt{2}$. The effect of dispersion during pulse propagation results in lengthening or compression of the pulse. In normal GVD regime ($g > 0$), group velocity decreases with frequency, i.e., redder frequencies travel faster than bluer ones, thus if $C > 0$ the pulse will become longer during the propagation. If $C < 0$ instead, the pulse will be initially compressed until the different frequencies are in phase and the pulse acquires its minimum possible duration (T_{min}) corresponding to the Fourier transform

limited case. This minimum pulse duration occurs at a distance x_{min}. In the case of anomalous GVD regime ($g<0$), when bluer frequencies travel faster than redder ones, the pulse gets longer for $C<0$ and is initially compressed if $C>0$ (compression is obtained whenever C and g have different signs).

The minimum pulse duration, T_{min}, and the corresponding distance inside the crystal, x_{min}, are obtained from Eq. (5)

$$x_{\min}=\frac{CL_D}{1+C^2} \quad \text{and} \quad T_{\min}=\frac{T_o}{\sqrt{1+C^2}}. \tag{6}$$

Taking into account that the GVD coefficient of SBN at 790 nm is $g=466\ fs^2/mm$ (calculated from SBN data in Ref. 14), it is clear from the previous considerations that down-chirped pulses will be compressed during propagation inside the SBN crystal. The experimental determination of x_{min} and the pulse duration FWHM in intensity, τ_{min}, give the value of initial chirp, C, and initial pulse duration (FWHM), τ_0, as follows:

$$C=\frac{4\ln(2)gx_{\min}}{1+C^2} \quad \text{and} \quad \tau_o=\sqrt{\tau_{\min}^2+\left(\frac{4\ln(2)gx_{\min}}{\tau_{\min}}\right)^2}. \tag{7}$$

Experiments have been performed using a laser source emitting pulses with durations down to 30 fs (Femtopower PRO HE CEP from Femtolaser) at a repetition rate of 1 kHz and with 2 mJ energy per pulse, operating at a central wavelength of 790 nm and a bandwidth of 40 nm (FWHM). The same system could deliver also shorter pulses, down to 6 fs, by means of hollow core post-compression technique[16] using Ne as gas with spectral phase compensation performed using chirped mirrors. To record the TSHG trace, we used a Spiricon SP620U CCD camera with 4 μm pixel size. The imaging system was arranged to provide the largest possible image of the relevant area of the crystal on the CCD. The intersecting angle between both beams was $2\alpha_{ext}=6.8°$. Before entering our setup and in order to test different initial conditions, the laser pulses with initial pulse duration around 30 fs at FWHM were phase modulated with a selected initial chirp using an acousto-optic device (Dazzler from Fastlite). We selected different negative values for the initial chirp C in order to obtain pulse compression at different propagation distances inside the crystal. For increasing values of the parameter |C|, the compression distance inside the crystal and the initial pulse duration increases.

As stated previously, the TSHG generated by the SBN crystal comprises three different contributions. To extract the AC signal from the background originating from the SH emission of each individual beam, we delayed temporally one pulse with respect to the other, so they would not overlap. In this way, we obtained only the two individual SH contributions. This signal, representing the background, was subtracted from the total one (when both pulses overlapped) leading to significant increase of signal to background ratio in the AC trace.

Figures 2(a)–2(f) show the experimental recorded images corresponding to the transverse AC trace along the crystal for different input conditions (the pulse was propagating from bottom ($x=0$) to top). Each image corresponds to a different value of initial chirp (varied experimentally in steps of $GDD=500\ fs^2$) and initial pulse duration. The compression and broadening effect of the AC trace during propagation in the 10 mm SBN crystal is clearly visible. Since the pulse spectrum was not modified by the Dazzler system, the pulse duration at the minimum width position is similar for all cases and represents a transform limited pulse if the introduced Dazzler phase is exactly compensated by the material dispersion (i.e., including all the dispersive orders). Typical AC traces, at the position of minimum pulse duration, x_{min}, (red) and in another point within the crystal (blue), are shown as insets of Figures 2(f) and 2(l). The measurement of the FWHM width of this AC trace, Δz_{FWHM}, gives the pulse duration from Eq. (2).

The evolution of the pulse duration inside the SBN crystal is shown in Figure 3 (left) for the different initial conditions. The maximum compression distance, x_{min}, and pulse duration at this point, τ_{min}, are the experimental data from which we obtain the values for chirp parameter, C, and initial

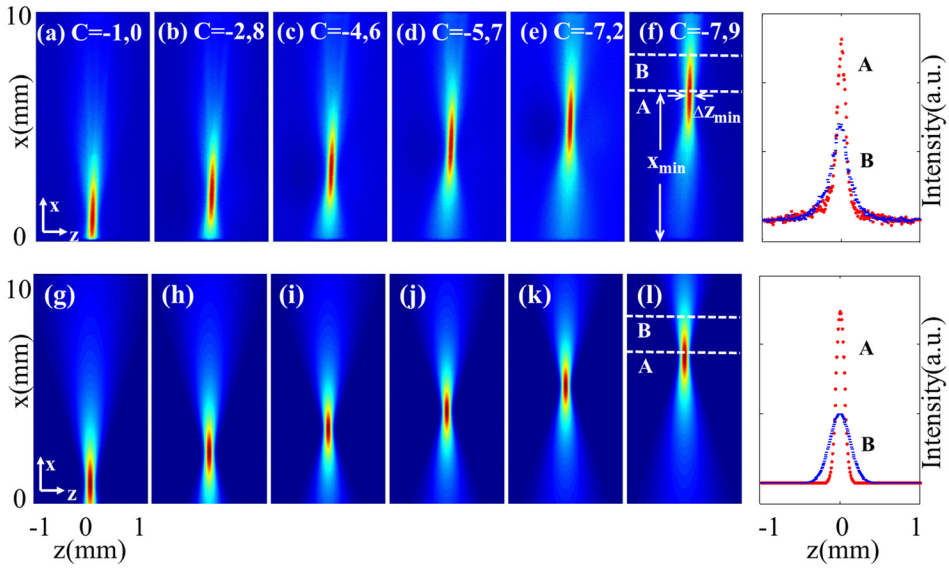

FIG. 2. Top: experimental recorded images of the AC trace along the SBN crystal for increasing |C| values from left to right side of the image. Bottom: Simulated AC traces of the pulses with the initial conditions determined from the experimental results (all situations correspond to initially down-chirped pulses $C<0$). Insets show the autocorrelation traces at the position A, corresponding to x_{min}, and B in (f) and (l).

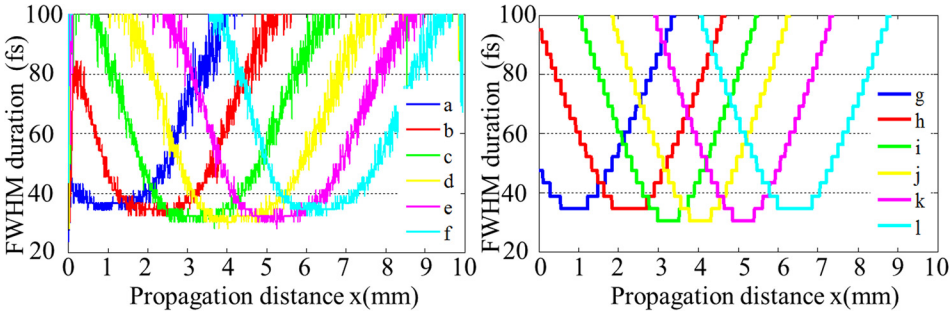

FIG. 3. Experimental data (left) and numerical simulations (right) of the temporal pulse evolution during the propagation inside the SBN crystal. Increasing |C| the maximum compression distance x_{min} is larger but τ_{min} is the same. The labels in the legend correspond to those in Figure 2.

pulse duration, τ_o, using Eq. (7). From these measurements, summarised in Table I, we can observe that the pulse duration at the maximum compression point is of the order of 30 fs in all cases. Notice that the value of τ_o could be also obtained by measuring the pulse duration directly at the entrance of the crystal but, since the temporal broadening of such short pulses along the 10 mm path is quite large, an accurate measurement of the pulse duration at this point would require the use beams broader enough to provide complete overlap along the crystal length.[11] However, with our proposed method, this condition can be relaxed since overlapping of the pulses is required just close to the maximum compression position.

In order to check the validity of the experimental results obtained with this simple method, we independently characterized the pulses using a standard SPIDER configuration and we found a very good correspondence between the results. The difference in the pulse duration obtained with both methods has not exceeded 2%. This difference is consistent with the resolution error introduced by our experimental setup taking into account the parameters of the CCD camera, the intersection angle α, and the propagation errors in the formulas (6) and (7). For the parameters used in our experiment, we obtained an error estimation of around 5% for the pulse duration and of the order of 10% for the chirp determination. The total error in the measurement would be larger due to intrinsic instabilities present in the pulse train.

In addition to experimental studies, we analyzed the evolution of the pulses using numerical simulations. To this end, we extended the numerical code introduced in Ref. 7 to include the initial chirp of the pulses and run a number of simulations using as initial parameters C and τ_o derived from the experimental results. The resulting numerically calculated AC traces are shown in Figures 2(g)–2(l), which correspond, respectively, to the experimental results (a)–(f). The numerically calculated values of the maximum compression distance, x_{min}, and pulse duration at this point (FWHM), τ_{min}, are shown in Table I. Again, very good agreement with experimental data is obtained. In order to check the contribution due to third-order effects, we included them (for SBN crystal, $\beta_3 = 360$ fs^3/mm at 790 nm) in the simulation. We have observed that for our pulse durations and propagating distances, they do not play any significant role.

The curves of the evolution of the pulse duration inside the SBN crystal obtained numerically are shown in Figure 3 (right) for comparison with the experimental results.

From the comparison between experimental and simulation values summarized in Table I, we see that our technique works well for pulse durations below 50 fs, since in this regime the dispersion properties of SBN allow for a dynamic behavior of the pulse measurable along the 1 cm length of our crystal. Additionally, the technique provides the opportunity for a real-time check the chirp content of a given pulse. The portable character of the setup makes possible to study the parameters of the pulse at any relevant location within a setup thus allowing for a real time optimization of the pulse characteristics.

We wanted to test the limitations of the technique performing similar measurements with pulses of decreasing durations. Before entering in our system, the pulses were carefully characterized using the d-scan technique[15] and FROG. As an example, we show a 13 fs (FWHM) pulse measurement where our experimental results (Fig. 4) show instead pulse durations longer than 20 fs.

Several factors can influence the resolution of our technique at these pulse durations such as pulse background subtraction errors due to pulse instabilities, resolution of the CCD camera, precision in the angle α measurement, nonGaussian temporal profile, or appearance of higher order dispersion effects. We studied the third-order dispersion, TOD, effect of the SBN crystal coefficient and observed a clear influence for pulses with durations shorter than 5 fs.

TABLE I. Experimental data corresponding to situations (a)–(f) in Figure 2 and retrieved values of C, GDD, and τ_0 (FWHM). Results retrieved from numerical simulation considering the calculated values as initial conditions corresponding to the plots (g)–(l) in Figure 2.

Experimental data			Calculated values			Simulation data		
	x_{min} (mm)	τ_{min} (fs)	C	τ_0 (fs)	GDD (fs^2)		x_{min} (mm)	τ_{min} (fs)
(a)	0.9	34	1.0	48	−410	**(g)**	0.89	35
(b)	2.3	32	2.8	96	−1050	**(h)**	2.27	34
(c)	3.2	30	4.6	142	−1510	**(i)**	3.26	30
(d)	4.0	30	5.7	175	−1880	**(j)**	4.02	30
(e)	5.1	30	7.2	220	−2380	**(k)**	5.12	35
(f)	6.4	32	7.9	257	−2980	**(l)**	6.42	35

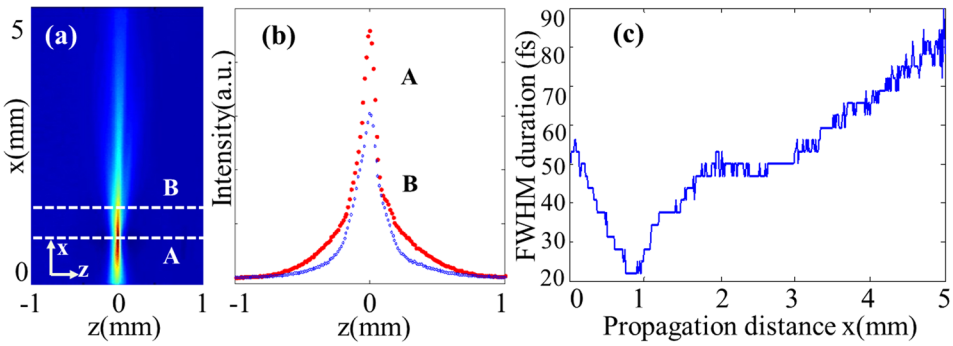

FIG. 4. (a) 13 fs pulse propagation along the SBN crystal recorded by a CCD camera. (b) AC trace at positions A and B and (c) pulse duration evolution during this propagation.

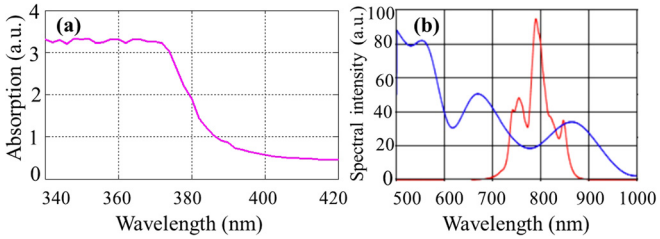

FIG. 5. (a) Plot of SBN crystals absorption versus the emitted wavelength. (b) Spectrum of the 13 fs pulse obtained by d-scan reconstruction.

Although these effects can be relevant for the resolution loss, they can be handled in the experimental conditions, and we do not consider that they can provide such a large discrepancy between the real and measured pulse durations.

The factor limiting the validity of the technique in this case is, to our opinion, the absorption window of the SBN crystal. In order to study this effect, we measured the absorption for the SBN crystals Figure 5(a) used in the experiments obtaining the absorption edge around $\lambda = 380$ nm, the wavelengths below that being absorbed by the SBN crystal. Measurement of the spectrum of the 13 fs pulses used, retrieved through the d-scan technique and shown in Figure 5(b), shows a central wavelength at $\lambda = 790$ nm, so approximately the lower half of the TSHG signal generated will be absorbed by the SBN crystal.

We checked this fact by using a reconstruction of the AC signal from the recorded spectrogram of the pulse, retrieved using a FROG system. Elimination of the lower part contribution of the spectrogram, corresponding to the part of the spectrum absorbed by the crystal, shows a broadening of the AC signal which is compatible with our observed results. We will explore in detail the effects of the absorption in a future work.

In conclusion, we have demonstrated that our simple pulse characterization technique based on transverse second harmonic generation can be used to measure chirp and pulse duration for pulses in the 30 fs regime. Even though we considered here the case of Gaussian pulses, our technique will work also for other pulse profiles, knowing how they evolve inside the SBN crystal. Our method works for any fundamental wavelength within the transparency window of SBN without need of further alignment. This setup can be also used for real-time monitoring of the chirp content at the measurement position. For the wavelengths corresponding to the anomalous GVD region, $g < 0$ ($\lambda > 2\,\mu$m for SBN), one should observe pulse compression for up-chirped pulses instead of down-chirped pulses as in the case discussed here.

We acknowledge financial support by Spanish Ministerio de Educación y Ciencia and European FEDER (Projects FIS2011-29734-C02-01 and FIS2013-44174-P), U.S. ACQRDECOM Project W911NF-12-1-0201, Generalitat de Catalunya (2009 SGR 1168), and Australian Research Council. We acknowledge Professor Helder Crespo for his support with the d-scan measurements. CLPU is acknowledged for granting access into its facility.

[1]I. Walmsley and C. Dorrer, Adv. Opt. Photonics **1**, 308 (2009).
[2]C. Iaconis and I. A. Walmsley, Opt. Lett. **23**, 792 (1998).
[3]R. Trebino, K. W. DeLong, D. N. Fittinghoff, J. N. Sweetser, M. A. Krumbügel, and D. J. Kane, Rev. Sci. Instrum. **68**, 3277 (1997).
[4]D. J. Kane and R. Trebino, IEEE J. Quantum Electron. **29**, 571–579 (1993).
[5]B. Alonso, I. J. Sola, Ó. Varela, J. Hernandez-Toro, C. Mendez, J. San Román, A. Zaïr, and L. Roso, J. Opt. Soc. Am. B **27**, 933 (2010).
[6]P. Bowlan, P. Gabolde, A. Shreenath, K. McGresham, R. Trebino, and S. Akturk, Opt. Express **14**, 11892 (2006).
[7]S. Kawai, T. Ogawa, H. S. Lee, R. C. DeMattei, and R. Feigelson, Appl. Phys. Lett. **73**, 768 (1998).
[8]A. R. Tunyagi, M. Ulex, and K. Betzler, Phys. Rev. Lett. **90**, 243901 (2003).
[9]V. Roppo, K. Kalinowski, Y. Sheng, W. Krolikowski, C. Cojocaru, and J. Trull, Opt. Express **21**, 25715 (2013).
[10]W. Wang, K. Kalinowski, V. Roppo, Y. Sheng, K. Koynov, Y. Kong, C. Cojocaru, J. Trull, R. Vilaseca, and W. Krolikowski, J. Phys. B: At., Mol. Opt. Phys. **43**, 215404 (2010).
[11]J. Trull, S. Saltiel, V. Roppo, C. Cojocaru, D. Dumay, W. Krolikowski, D. Neshev, R. Vilaseca, K. Staliunas, and Y. S. Kivshar, Appl. Phys. B **95**, 609 (2009).
[12]J. Janzsky, G. Corradian, and R. N. Gyuzalian, Opt. Commun. **23**, 293 (1977).
[13]J.-C. Diels and W. Rudolph, *Ultrashort Laser Pulse Phenomena*, 2nd Edition (Academic Press, San Diego, 2006).
[14]Th. Woike, T. Granzow, U. Dörfler, Ch. Poetsch, W. Wöhlecke, and R. Pankrath, Phys. Status Solidi **186**, R13–R15 (2001).
[15]M. Miranda, T. Fordell, C. Arnold, A. L'Huillier, and H. Crespo, Opt. Express **20**, 688 (2011).
[16]M. Nisoli, S. DeSilvestri, and O. Svelto, Appl. Phys. Lett. **68**, 2793 (1996).